



Composite Flywheel Development for Energy Storage

by Jerome Tzeng, Ryan Emerson, and Paul Moy

ARL-TR-3388

January 2005

NOTICES

Disclaimers

The findings in this report are not to be construed as an official Department of the Army position unless so designated by other authorized documents.

Citation of manufacturer's or trade names does not constitute an official endorsement or approval of the use thereof.

Destroy this report when it is no longer needed. Do not return it to the originator.

Army Research Laboratory

Aberdeen Proving Ground, MD 21005-5066

ARL-TR-3388

January 2005

Composite Flywheel Development for Energy Storage

Jerome Tzeng, Ryan Emerson, and Paul Moy
Weapons and Materials Research Directorate, ARL

Report Documentation Page

Form Approved
OMB No. 0704-0188

Public reporting burden for this collection of information is estimated to average 1 hour per response, including the time for reviewing instructions, searching existing data sources, gathering and maintaining the data needed, and completing and reviewing the collection information. Send comments regarding this burden estimate or any other aspect of this collection of information, including suggestions for reducing the burden, to Department of Defense, Washington Headquarters Services, Directorate for Information Operations and Reports (0704-0188), 1215 Jefferson Davis Highway, Suite 1204, Arlington, VA 22202-4302. Respondents should be aware that notwithstanding any other provision of law, no person shall be subject to any penalty for failing to comply with a collection of information if it does not display a currently valid OMB control number.
PLEASE DO NOT RETURN YOUR FORM TO THE ABOVE ADDRESS.

1. REPORT DATE (DD-MM-YYYY) January 2005			2. REPORT TYPE Final		3. DATES COVERED (From - To) November 2002–October 2003	
4. TITLE AND SUBTITLE Composite Flywheel Development for Energy Storage					5a. CONTRACT NUMBER	
					5b. GRANT NUMBER	
					5c. PROGRAM ELEMENT NUMBER	
6. AUTHOR(S) Jerome Tzeng, Ryan Emerson, and Paul Moy					5d. PROJECT NUMBER 622618H75	
					5e. TASK NUMBER	
					5f. WORK UNIT NUMBER	
7. PERFORMING ORGANIZATION NAME(S) AND ADDRESS(ES) U.S. Army Research Laboratory ATTN: AMSRD-ARL-WM-MB Aberdeen Proving Ground, MD 21005-5066					8. PERFORMING ORGANIZATION REPORT NUMBER ARL-TR-3388	
9. SPONSORING/MONITORING AGENCY NAME(S) AND ADDRESS(ES)					10. SPONSOR/MONITOR'S ACRONYM(S)	
					11. SPONSOR/MONITOR'S REPORT NUMBER(S)	
12. DISTRIBUTION/AVAILABILITY STATEMENT Approved for public release; distribution is unlimited.						
13. SUPPLEMENTARY NOTES						
14. ABSTRACT Composite flywheels for energy storage have been proposed and investigated for the past several decades. Successful applications are, however, limited due to the inability to predict the performance, especially the long-term durability. In this investigation, a comprehensive study was proposed with the intent to implement composites in high-performance flywheels. The potential failure mechanism of flywheels constructed with fiber composites was evaluated. Analytical codes for predicting elastic and viscoelastic (long-term) behavior were developed for flywheel design. Material characterization and test matrices were proposed to design flywheels with maximum performance. Component-level test methods and devices were developed to validate flywheel performance. Finally, a methodology incorporating these studies is presented for the design and manufacture of composite flywheels.						
15. SUBJECT TERMS composite flywheel, filament winding, viscoelasticity, rotor strain measurement						
16. SECURITY CLASSIFICATION OF:			17. LIMITATION OF ABSTRACT	18. NUMBER OF PAGES	19a. NAME OF RESPONSIBLE PERSON Jerome T. S. Tzeng	
a. REPORT UNCLASSIFIED	b. ABSTRACT UNCLASSIFIED	c. THIS PAGE UNCLASSIFIED			19b. TELEPHONE NUMBER (Include area code) 410-306-0959	

Standard Form 298 (Rev. 8/98)
Prescribed by ANSI Std. Z39.18

Contents

List of Figures	iv
1. Introduction	1
2. Analytical Models	3
3. Material Testing	7
4. Rotor Testing: Vibration and Strain Measurement	9
4.1 Improvements to ARL OESM System.....	11
4.2 Pattern Shape.....	11
4.3 Pattern Application.....	12
4.4 Sensor Geometry	12
4.5 Configuration and Control of the Sensor	12
4.6 OESM System at ARL	12
5. Conclusion	13
6. References	14
Distribution List	15

List of Figures

Figure 1. Definition of coordinate systems and stress components in a rotating cylinder.	2
Figure 2. Stress profile in a hoop-wound composite cylinder with 3-in inner and 6-in outer radii, subjected to 50,000-rpm rotational load.	2
Figure 3. Composite time-dependent unit ply properties. Transverse and shear properties are time-dependent and expressed with power forms.	5
Figure 4. Decrease of the preload (radial stress at 4.5-in radius) at the interface of a pressfit assembly due to creep and stress relaxation of composite.	5
Figure 5. Change of the radial stress profile in a rotating wheel due to creep and stress relaxation of composite.	6
Figure 6. Change of the hoop-stress profile in a rotating wheel due to creep and stress relaxation of composite.	6
Figure 7. Twenty-inch diameter composite cylinders fabricated at ARL facilities.	7
Figure 8. Iosipescu test specimen represents the loading condition and rotor construction. Shear strength increases as the glass content increases.	8
Figure 9. Fracture increases as the glass fiber content increases in the composite laminate. The glass is oriented to arrest the crack propagation.	9
Figure 10. Illustration of a pattern and sensor configuration with corresponding duty cycle (10).	10
Figure 11. Illustration of change in duty cycle at one radial location before and after deformation (10).	10
Figure 12. Illustration of a four-lobe linear boundary and four-lobe spiral boundary pattern.	11
Figure 13. Picture of the rotor testing facility at ARL.	13

1. Introduction

Composite flywheels are currently being developed for energy storage. The energy stored in the flywheel can be retrieved to supply power for electrical-drive machinery. To satisfy the high-performance and low-weight constraints, high-strength carbon fiber composites are the materials of choice for flywheel construction. Recently, several composite flywheels have been developed for commercial power generation and vehicles such as buses and trains. In the government sector, National Aeronautics and Space Administration (NASA) intends to have composite flywheels in the space station for energy storage. Flywheels have also been proposed for satellite attitude control. There are investigations of hybrid and all-electric combat vehicles and weapons. Composite flywheels are crucial components of the systems. There have been numerous research and development (R&D) programs on composite flywheels in the past (1–3). Several programs have been conducted in National Laboratories for nuclear applications. Some long-term programs were performed in academia and industry. In spite of much effort, few successful composite flywheels have been built and used in practical applications. The shortcomings that hinder the use of composite materials in flywheel applications will be illustrated and discussed. A new approach for design and testing is also proposed in the following sections.

The inertial stresses in a flywheel during operation (high-speed rotation) are dominant in the circumferential direction and, consequently, composite flywheel rotors are usually filament wound with the fiber reinforcements oriented in this direction. However, tensile stress is also developed in the radial direction due to mismatches in the growth of the rotor as well as Poisson effects. Because filament wound composite rotors lack reinforcement through the radial thickness, these rotors generally fail by radial delamination prior to fiber breakage in the circumferential direction. An elastic thick-walled composite cylinder analysis was developed to determine the stress and strain profiles in a flywheel. Figure 1 shows the definition of stress components and coordinate systems used in the analysis. Figure 2 illustrates the stress profile in a graphite composite cylinder with 3-in and 6-in inner and outer radii, respectively, subjected to 50,000 rpm rotational load. As shown in the analysis, the maximum hoop stress is ~95 ksi and is below the strength limit. However, the radial stress in this case is ~10 ksi—far exceeding the strength in that direction. These stresses were calculated using the model developed in reference (4).

By assembling the rotor with a press fit or shrink fit, compressive radial stress is built-in, which helps to mitigate the radial stresses that develop during operation. Consequently, higher rotor performance is realized by avoiding premature failure by radial delamination. The press fit process, however, might induce significant banding and shear stresses along the axial direction of the cylinder during fabrication. Axial reinforcement might therefore be needed for a flywheel

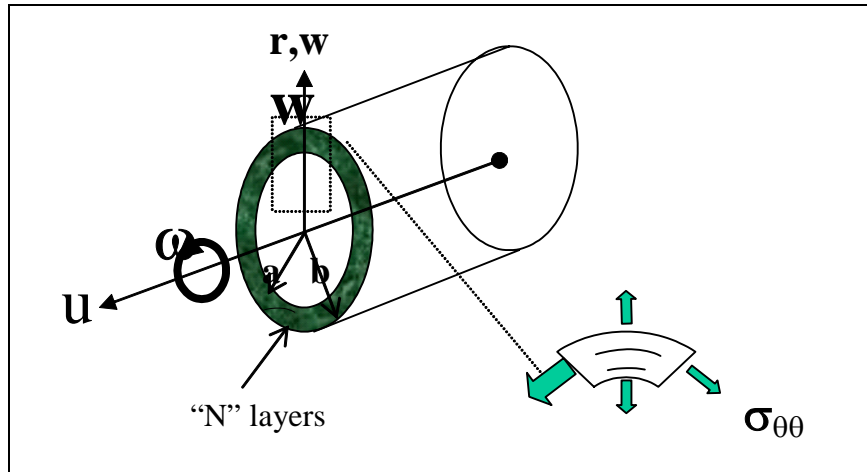


Figure 1. Definition of coordinate systems and stress components in a rotating cylinder.

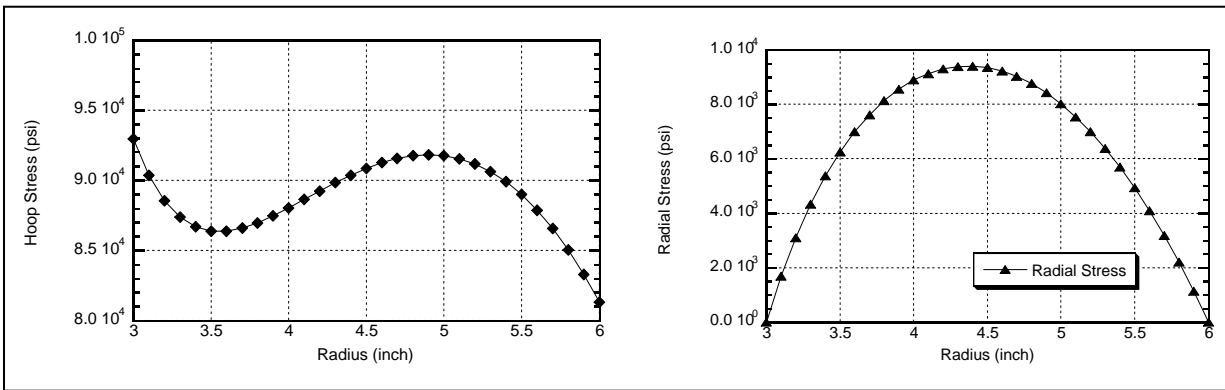


Figure 2. Stress profile in a hoop-wound composite cylinder with 3-in inner and 6-in outer radii, subjected to 50,000-rpm rotational load.

to achieve a higher speed or performance. With this in mind, a series of material tests were performed to determine the tensile and shear properties of laminates in this investigation. The test results will be used to design the layup of a composite rotor subjected to various loading conditions, including those induced by the manufacturing processes.

To achieve high performance, the stresses in a composite rotor must be high during operation. Accordingly, the long-term behavior of the composite materials used in flywheel rotors is particularly critical. Over time, the stress and strain profiles can change in a composite flywheel significantly affecting the structural performance. Creep and fatigue crack growth are durability

concerns that lead to unbalance in the rotor. To assist in evaluating the occurrence of such time-dependent phenomena, a viscoelastic analysis of flywheels was developed. Fracture properties of the composite laminates of interest were also evaluated in conjunction with the potential crack growth and failure mechanism (5).

The rotor deformation needs to be monitored in order to validate structural design and integrity. Currently, deformation of a rotating body can be measured by strain gage with a split ring at the spindle or a laser measurement. The strain gage works only up to a moderate speed then fails because of high centripetal force. The traditional laser device basically measures the distance change between the rotor surface and the device location. However, neither method will be able to satisfy the measurement required of a high-speed rotor. A noncontact optical-sensing technique was developed during the investigation. The method will enable a real-time monitor of rotor conditions and will be discussed in detail.

Recent flywheel developments for energy storage of U.S. Army electric weapons and hybrid vehicles are discussed in this report. Technologies to achieve high-performance composite flywheels were developed during the course of this study. In the following section, those technologies will be presented, including analytical models, material characterization, component spin tests, and flywheel life assessment.

2. Analytical Models

An analytical model is necessary to predict creep and preload loss due to the time-dependent behavior of composites. A viscoelastic analysis has been developed that is relevant for thick-walled composite cylinders (6, 7). The Boltzmann superposition integral is used for the complete spectrum of increments of anisotropic material constants with respect to time. In the analysis, a thick composite cylinder is assumed to remain at a constant elevated temperature, and all boundary conditions are independent of time. Accordingly, the linear thermal viscoelastic problem can be derived from the associated linear elastic problem by employing the elastic/viscoelastic correspondence principle. In other words, the integral constitutive equations reduce to algebraic relations, which are essentially identical to those developed for elastic media when they are Laplace transformed by means of the rule for convolution integrals. The elastic analysis can thus be used to derive the transformed viscoelastic solutions in the time domain.

The coordinate system used to model a rotor is shown in figure 1. The governing equation can be derived from the momentum equation with anisotropic constitutive material properties as follows:

$$r^2 \frac{d^2 \bar{w}}{dr^2} + r \frac{d \bar{w}}{dr} - \bar{\lambda}^2 \bar{w} = \frac{(\tilde{C}_{13} - \tilde{C}_{12})}{s \tilde{C}_{33}} \varepsilon^o r - \frac{\rho \omega^2}{s \tilde{C}_{33}} r^3, \quad (1)$$

where w is radial displacement and r is radius, ω is angular velocity, ε is axial elongation, and s denotes the Laplace transform variable. The C_{ij} terms are material properties (4).

Equation 1 is the governing equation in the Laplace domain. Here and henceforth, an overbar denotes functions of the Laplace transform variable. The elastic formulation has a similar form according to the correspondence principle. While this equation can represent any composite layer (with one set of material properties) within a multiple-layer composite cylinder, properties are allowed to vary from layer to layer.

Solving equation 1 for \bar{w} yields the complete solution as follows:

$$\bar{w} = \bar{A}_1 r^{\bar{\lambda}} + \bar{A}_2 r^{-\bar{\lambda}} + \tilde{w}_p, \quad (2)$$

where \bar{A}_1 and \bar{A}_2 are coefficients determined from boundary and continuity conditions. The particular solution is obtained in the following expression:

$$\tilde{w}_p = \frac{\tilde{C}_{12} - \tilde{C}_{13}}{\tilde{C}_{33} - \tilde{C}_{22}} \varepsilon r - \frac{1}{9 - \bar{\lambda}^2} \frac{\rho \omega^2}{\tilde{C}_{33}} r^3. \quad (3)$$

A set of simultaneous equations can be assembled for a multiple-layer composite cylinder. The total number of equations is determined by the number layers in the cylinder. A numerical technique was developed, which applies the continuity boundary condition during the assembly process of the equation set (6). This process reduces the total number of the equations to one half. Finally, traction-boundary conditions are applied to the assembly of equations that comprise the multiple-layer cylinder.

The analysis previously described is used to simulate a composite press fit assembly. The simulation is composed of two concentric cylinders. The inner cylinder has a 3-in inner radius and a wall thickness of 1.5 in. The outer cylinder has a 4.5-in inner radius and also has a wall thickness of 1.5 in. Both cylinders are hoop wound and constructed of graphite/epoxy composite. The shear and transverse material properties (compliances) are treated as time dependent, and are given in figure 3. The fiber direction compliance and Poisson's ratios are assumed to be elastic.

Figure 4 shows that the preload at the interface of cylinders decreases over a period of time. Stress relaxation is observed in the initial preload (radial stress at the interface between the inner and outer cylinders), which decreases over time from 5000 to 4000 psi. In response to this decrease in preload, it would be necessary to reduce the rotational speed of the rotor (i.e., knockdown the mechanical performance) because the preload is essential for preventing radial delamination. Figure 5 illustrates the change in the radial stress profile over a period of time for the flywheel subjected to constant rotation at 50,000 rpm. The hoop-stress profile changes also, as illustrated in figure 6. There is significant redistribution of stresses that should be considered in the design.

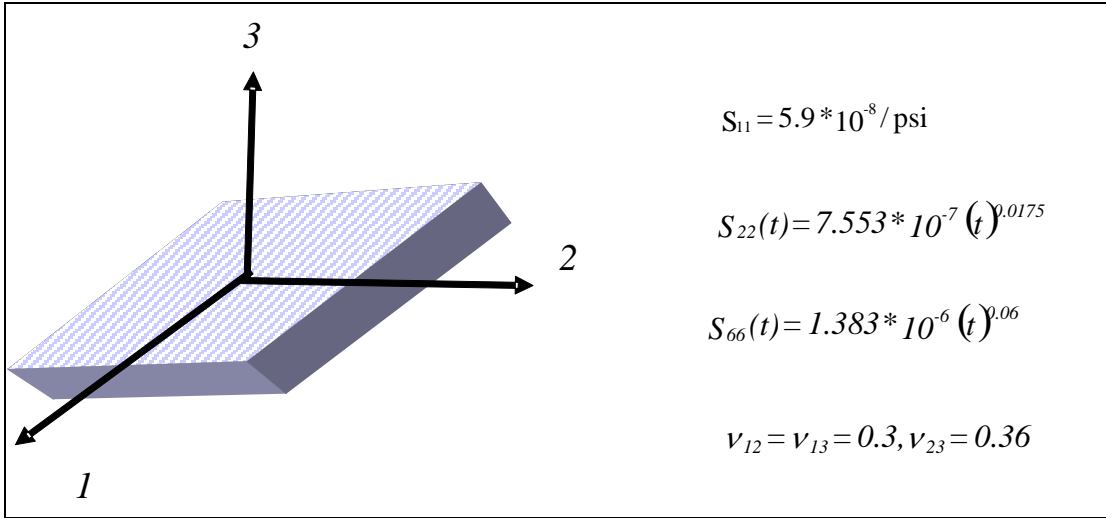


Figure 3. Composite time-dependent unit ply properties. Transverse and shear properties are time-dependent and expressed with power forms.

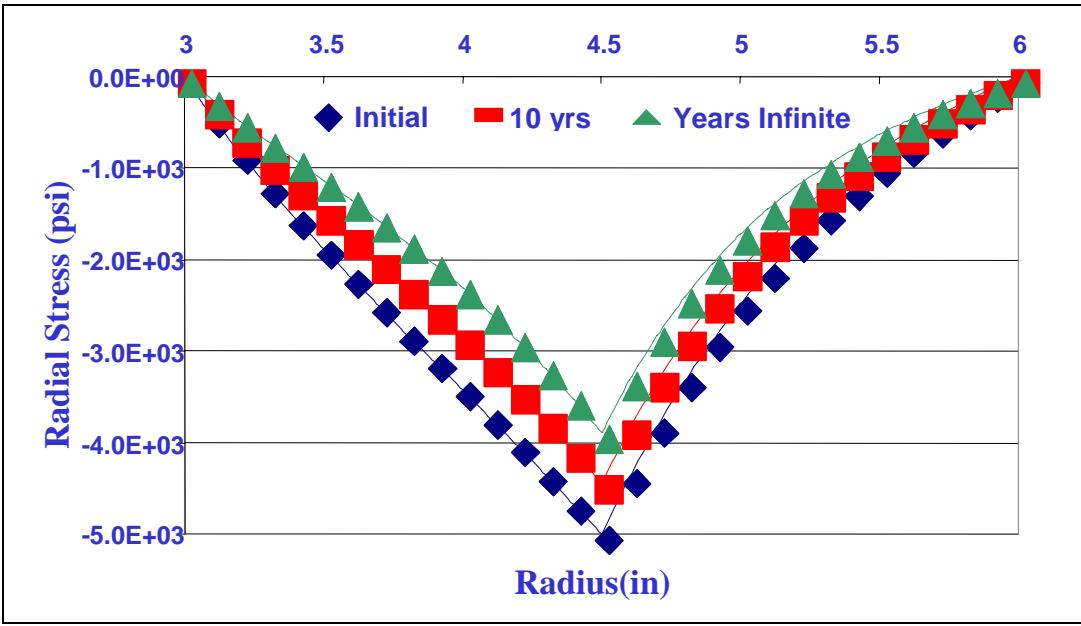


Figure 4. Decrease of the preload (radial stress at 4.5-in radius) at the interface of a pressfit assembly due to creep and stress relaxation of composite.

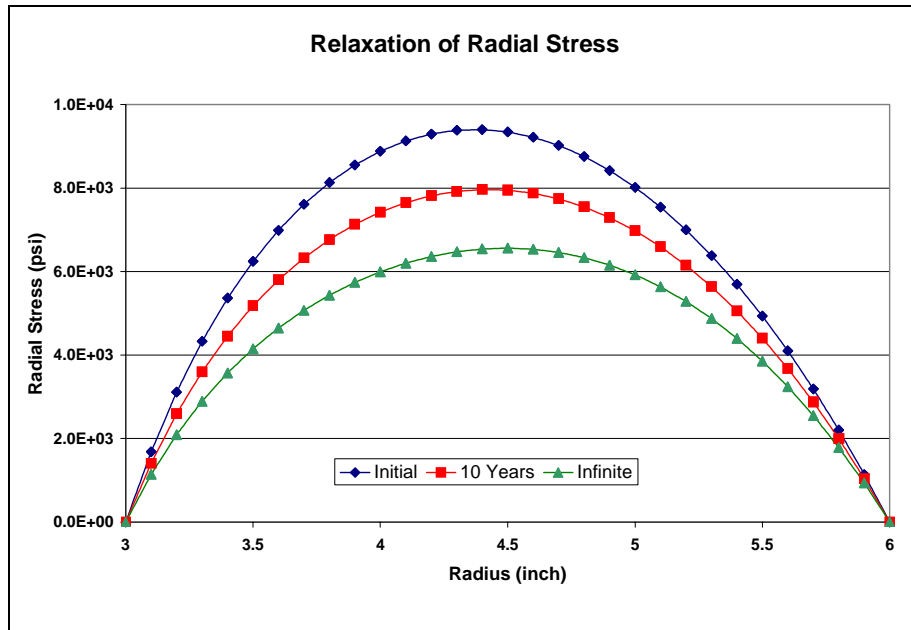


Figure 5. Change of the radial stress profile in a rotating wheel due to creep and stress relaxation of composite.

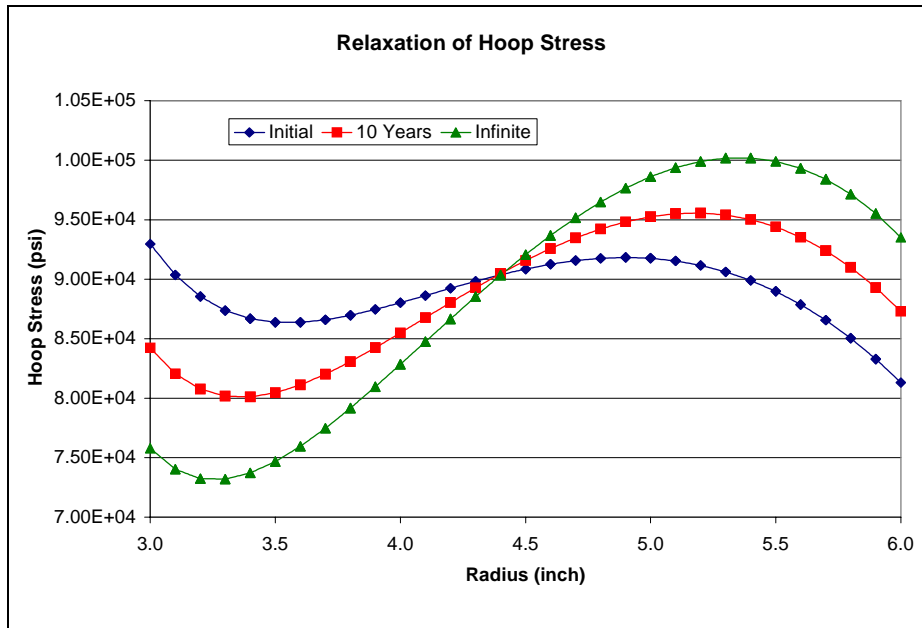


Figure 6. Change of the hoop-stress profile in a rotating wheel due to creep and stress relaxation of composite.

3. Material Testing

Composite cylinders with an inner diameter of 20 in were fabricated at the U.S. Army Research Laboratory (ARL) in-house facilities as shown in figure 7. David Spagnuolo, Robert Kaste, and Dennis Henry contributed to the fabrication of cylinders including mandrel fabrication, filament winding, and cure kinetics study. The details of manufacture will be documented in a separate report. The cylinder was made of T1000G graphite/epoxy composite. Several thin cylinders (0.1 in thick) were fabricated and sliced into 0.5-in-wide ring specimens for hydro-burst testing. A test matrix was conducted to measure the strength and stiffness of these composite ring specimens. This procedure works well for evaluating the circumferential strength of cylinders fabricated with various fiber volume fractions, matrix materials, and fabrication methods. High strength is obtained through careful engineering and manufacturing of the cylinders. The strengths measured from the ring samples were between 500 to 600 ksi for the fabrication methods and material systems used.



Figure 7. Twenty-inch diameter composite cylinders fabricated at ARL facilities.

As discussed previously, the performance of a composite flywheel can be enhanced through a proper laminate architecture design with axial reinforcements. A series of tests was performed to evaluate the enhancement of S-2 Glass* axial reinforcement on the transverse, shear, and fracture properties of laminates. Effects of glass ply content on shear strength were evaluated using carbon/glass hybrid laminates. T1000G composite laminates with various axial glass contents were tested using Iosipescu shear tests. Figure 8 shows the trend of the enhancement of shear strength (τ_{23}) of the T1000G laminate with increasing glass content. These results can be used in the design of laminated composite cylinders. An identical test matrix was also performed for transverse tensile tests.

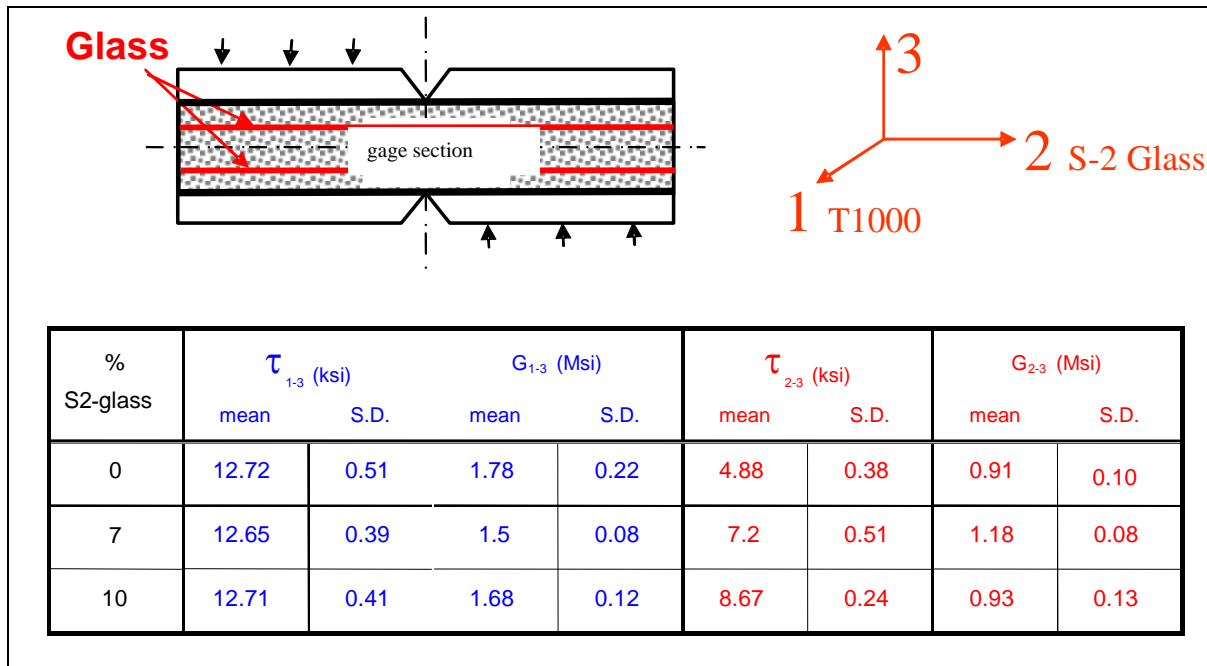


Figure 8. Iosipescu test specimen represents the loading condition and rotor construction. Shear strength increases as the glass content increases.

Fracture toughness is a critical property for composite flywheels subjected to a very high operating stress. Microcracks developed in the matrix can propagate and cause delamination in the rotor. A composite system with high fracture toughness has a slow rate of crack propagation and, thus, a longer fatigue life. The fracture toughness of composite cylinders can also be enhanced by adding glass content in the rotor axial direction (5). Figure 9 shows how the glass content affects the fracture toughness. Reference (8) gives details of the test method, results, and fracture mechanism predicted for composite cylinders. The dependence of loading rate on the fracture toughness is also evaluated, which is useful for a high-rate loading condition. In conjunction with this study, a fatigue study on combined shear and compressive loading of composite laminates was performed (9).

* S-2 Glass is a registered trademark of Owens Corning.

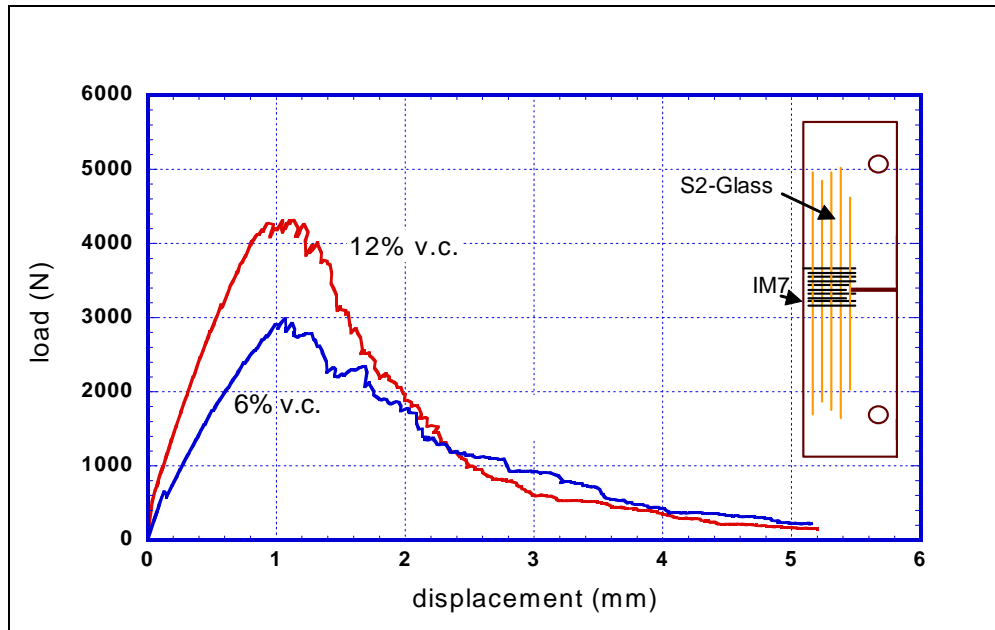


Figure 9. Fracture increases as the glass fiber content increases in the composite laminate. The glass is oriented to arrest the crack propagation.

4. Rotor Testing: Vibration and Strain Measurement

Several techniques exist for measuring strains in the rotors of flywheels during operation, including strain gages with slip rings or telemetry, x-ray diffraction, and optoelectronic strain measurement (OESM). The OESM technique (described in detail in references [10] and [11]) is capable of simultaneously measuring and isolating flexible-body displacements (strain) and rigid-body displacements (vibration) in a noncontact fashion on flywheels rotating at several tens of thousands of rpm. In addition, the computer control of the OESM sensor enables the displacements to be measured in a quasi-continuous fashion (i.e., without postprocessing), and the OESM technique includes built-in compensation for drift/aging of the sensor. The combination of these previously-mentioned features, as well as its compact size, makes the OESM technique suitable for long-term autonomous operation in the field.

The OESM technique consists of two components: a reflective pattern applied to the axial face of the flywheel, and a sensor that “looks at” the pattern as the flywheel rotates. The OESM sensor projects a stationary spot of light onto the axial face of a rotating disk. The reflective pattern on the axial face of the disk modulates the reflectivity of the light spot. This pattern, which deforms in unison with the disk, is designed such that the in-plane displacement of the disk is effectively “encoded” into a stream of reflected pulses of light. A photodetector on the sensor converts this stream of reflected light pulses to electrical pulses and sends these electrical pulses to the gate of a timer/counter circuit in a digital computer. The computer uses a

tachometer signal to convert the (temporal) pulse widths to angular widths of the reflective features of the pattern. Figure 10 shows an illustration of a rotor with inner and outer radii, r_i and r_o , respectively, with a pattern that has one reflective patch (the cardioid shape shown in white). Also shown in figure 10 is the corresponding swept-angle, ϕ , or so-called duty cycle, output from the sensor.

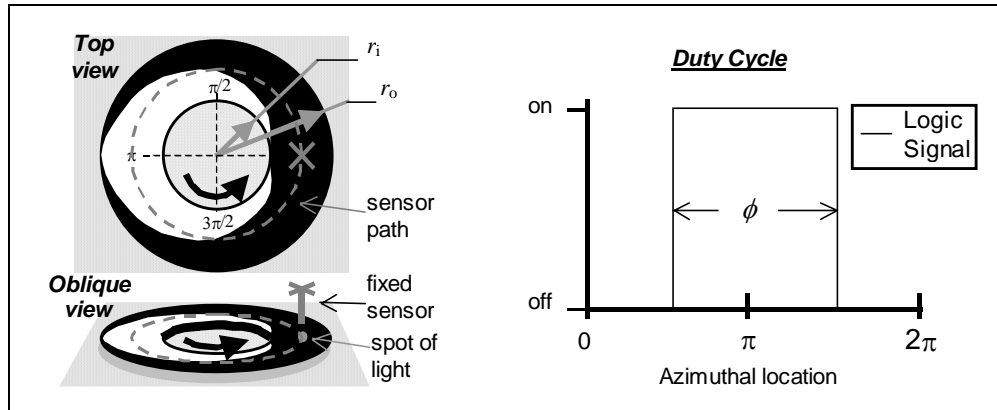


Figure 10. Illustration of a pattern and sensor configuration with corresponding duty cycle (10).

The instantaneous displacement, u , of the rotor at the location of the projected spot of light is determined by comparing the instantaneously measured angular widths to a calibration record of pulse width vs. radial location on the rotor. Figure 11 shows the duty cycle before deformation, ϕ_1 , and after deformation, ϕ_2 , for a sensor fixed in space at a location corresponding to an initial radial location r_1 on the under-formed rotor.

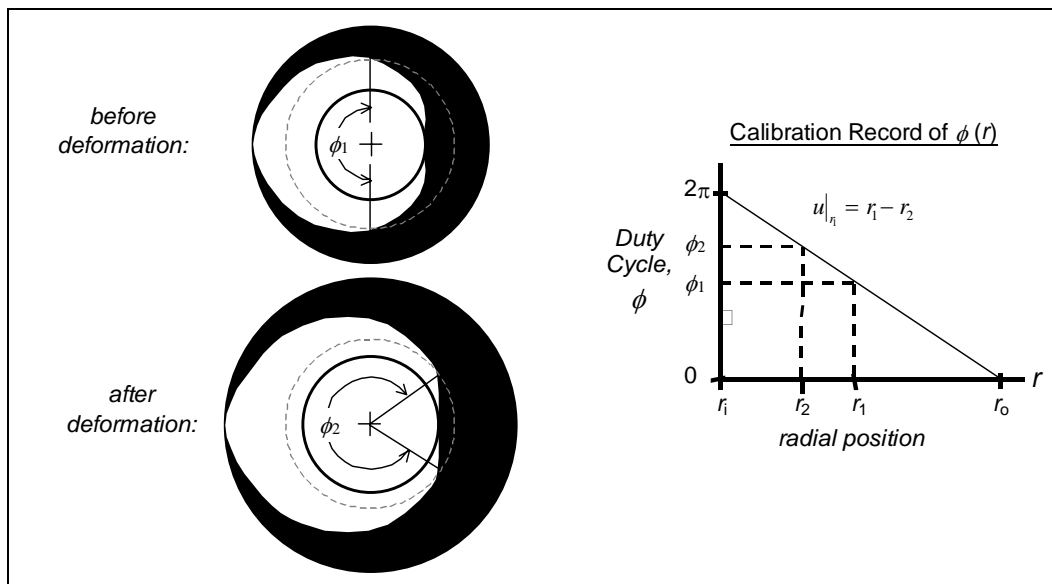


Figure 11. Illustration of change in duty cycle at one radial location before and after deformation (10).

4.1 Improvements to ARL OESM System

Recent changes have been made to many aspects of the OESM system since the original system was developed. These changes encompass improvements to the pattern shape, the technique for applying the pattern to the rotor, the sensor geometry, and configuration and control of the sensor.

4.2 Pattern Shape

While the shape of the pattern shown in figures 10 and 11 is a spiral boundary shape (10, 11), the pattern shape used in practice possessed geometric features with linear boundaries. Figure 12 shows a comparison of these two types of pattern shapes on an identical annular rotor. Note that the patterns shown in figure 12 possess four reflective lobes, while the patterns shown in figures 10 and 11 have only one lobe (for illustrative purposes).

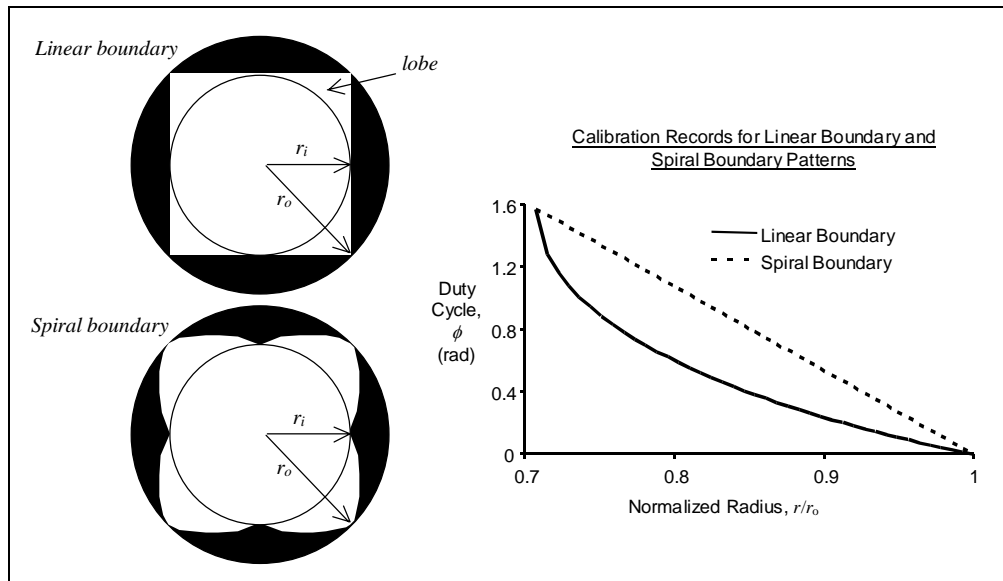


Figure 12. Illustration of a four-lobe linear boundary and four-lobe spiral boundary pattern.

A linear boundary pattern possesses a region near the inner radius where the duty cycle exhibits a large change with respect to radial position. This large change corresponds to a large “slope” of the calibration record and, therefore, is a pattern with favorable sensitivity to radial displacement (figure 12). It has been found, however, that the portion of the linear boundary pattern near r_i (where this large slope is an advantage) is not practical to use. In the usable radial locations in a linear boundary pattern, the duty cycle of a spiral boundary pattern exhibits equivalent or better sensitivity to radial displacement than a linear boundary pattern. The sensitivity of a linear boundary pattern quickly decays away from the inner radius, while the sensitivity of a spiral boundary pattern remains essentially constant over the entire radial region. Based on these findings, the current rotor-testing protocol employs a spiral boundary reflective pattern.

4.3 Pattern Application

The reflective pattern in the OESM system is essentially analogous to a strain gage in as much as the pattern must not significantly reinforce the rotor, and it must deform with the rotor. With the previous OESM technique, the pattern was applied to the axial face of the rotor with a spray-on photographic emulsion. The emulsion was developed in a contact-print fashion using a mask with computer-generated geometric features. The main drawbacks of this pattern application technique are that it is very laborious, and it results in a delicate pattern. The new technique for applying the reflective pattern uses a thin layer of reflective paint followed directly by a thin layer of ink that is applied using a pen and compass. The resulting pattern is able to be applied faster and is much more resistant to damage that may occur during handling of the rotor.

4.4 Sensor Geometry

During testing of the original OESM system, it was found that when the vertical distance between the rotor and the sensor changed more than $\sim 50 \mu\text{m}$, significant errors were introduced into the measurement of the apparent duty cycle. It is believed that some of this sensitivity was attributable to drifting of the spot in the active area of the photodetector, as the original OESM sensor projected the spot of light onto the rotor surface at an angle that was $\sim 10^\circ$ away from perpendicular. Also, the original sensor had a stand-off distance between the sensor and the rotor surface of $\sim 4.5 \text{ mm}$; thus, vertical displacements resulted in defocusing of the projected spot. With these design issues in mind, the current OESM sensor has a stand-off distance of $\sim 50 \text{ mm}$ and projects the light perpendicularly to the surface.

4.5 Configuration and Control of the Sensor

The OESM system described in references (10) and (11) was configured with 10 positions equally spaced along a radial line at which a sensor could be located. The sensors in this configuration remained stationary during operation. The displacements measured at these 10 locations, therefore, were only useful for constructing a rather coarse full-field “picture” of the state of strain in the rotor. The current OESM setup uses a single sensor, which is bolted to a linear stepper motor stage. The stroke length of this linear stage is capable of scanning a large radial range (125 mm) in radial increments as small as $1 \mu\text{m}$, thus enabling the construction of a very fine full-field “picture” of the state of strain in the rotor. Also, a new algorithm for controlling the inevitable drift of the sensor (12) will be employed in the current OESM system at ARL.

4.6 OESM System at ARL

Measurement of radial growth is an essential piece of data for validating the structural design and analysis of the flywheel rotor. It is unlikely that any rotor will be accepted for operation in the field without validation by testing. The previously developed OESM technique was capable of measuring displacements with $1\text{-}\mu\text{m}$ sensitivity on a disk rotating at 20 krpm. While not yet

fully tested, the improvements embodied in the current OESM system as previously described should enable a several-fold increase in the sensitivity to displacement. Figure 13 shows a picture of the spin test facility at ARL, which is ready to be used in the component tests in support of the efforts for developing a pulsed power rotating machine.

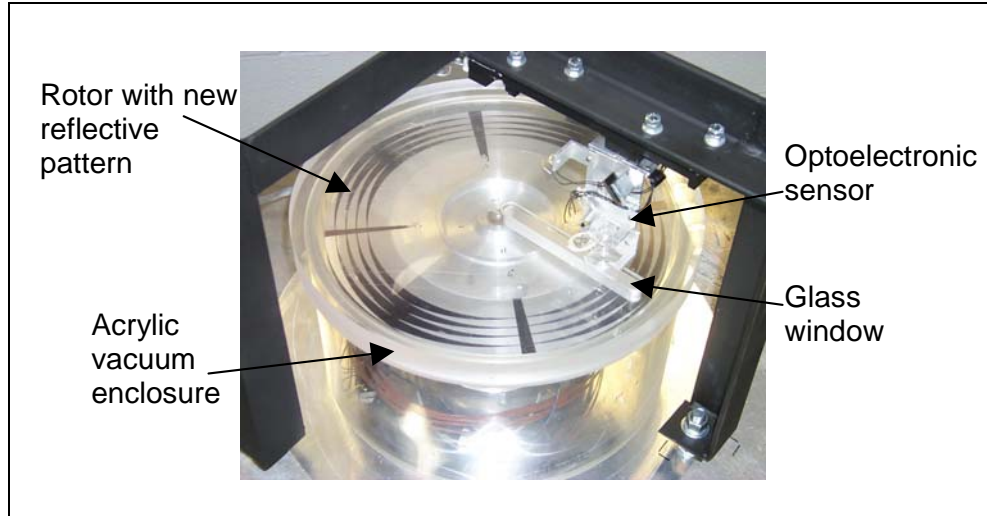


Figure 13. Picture of the rotor testing facility at ARL.

5. Conclusion

A comprehensive research program has been conducted to develop high-performance composite flywheels for energy storage applications. Modeling techniques including elastic, viscoelastic, and fatigue analyses were developed for design as well as prediction of rotor behaviors. A laminate architecture for achieving high mechanical performance of flywheels was proposed based on lessons learned from previous programs. A material test matrix at the laminate level was also proposed from a design point view of high-performance flywheels. The optical strain measurement technique can be used to validate flywheel design and construction. Particularly, the proposed design and test procedure indeed considers the long-term behavior of flywheel such as creep, stress relaxation, fatigue, and fracture of composites.

6. References

1. Stone, R. G. *Fiber-Composite Flywheel Program: Quarterly Progress Report*; UCRL-50033-76-4; Lawrence Livermore National Laboratory: Livermore, CA, 1976.
2. Pardoen, R.; Nudenberg, D.; Wartout, B. E. Achieving Desirable Stress States in Thick Rim Rotating Disks by Variation of Properties. *Proceedings of the 1980 Flywheel Technology Symposium 159*, Dayton, OH, October 1980.
3. Acebal, R. Energy Storage Capabilities of Rotating Machines Including a Comparison of Laminated Disk and Rim Rotor Design. *IEEE Transactions on Magnetics* **1999**, 35 (1).
4. Tzeng, J. T.; Chien, L. S. A Thermal/Mechanical Model of Axially Loaded Thick-Walled Composite Cylinders. *Journal of Composite Engineering* **1994**, 4 (2).
5. Tzeng, J. T.; Moy, P. Composite Rotor Design for Fatigue Crack Growth Resistance. *Proceedings of the 16th Technical Conference, American Society for Composites*, Blacksburg, VA, September 2001.
6. Tzeng, J. T. Viscoelastic Analysis of Composite Cylinder Subject to Rotation. *Journal of Composite Materials* **2002**, 36 (2) 229–239.
7. Tzeng, J. T. Viscoelastic Modeling of Press-Fitted Composite Cylinders. *Journal of Composite Technology and Research* **2001**, 23 (1), 21–27.
8. Moy, P.; Tzeng, J. T. Loading Rate Effect on Translaminar Fracture Toughness of Hybrid Composite Laminates; Dynamic Failure in Composite Materials and Structures AMD-Vol. 243, *ASME International Mechanical Engineering Congress & Exposition*, 5–7 November 2000.
9. DeTeresa, S. J.; Allison, L. M.; Freeman, D. C.; Groves, S. E. Matrix-Dominated Performance of Thick-Section Fiber Composite for Flywheel Applications. *Proceedings of SAMPE Technical Conference*, Long Beach, CA, May 2001.
10. Emerson, R. P. Viscoelastic Flywheel Rotors: Modeling and Measurement. Ph.D. dissertation, The Pennsylvania State University, University Park, PA, December 2002.
11. Emerson, R. P.; Bakis, C. E. Optoelectronic Strain Measurement for Flywheels. *Experimental Mechanics* **2002**, 42, 237–246.
12. Bakis, C. E.; Haldeman, B. J.; Emerson, R. P. Optoelectronic Radial Displacement Measurement Method for Rotating Disks. In *Recent Advances in Experimental Mechanics*; E. E. Gdoutos, Ed.; Kluwer Academic Publishers: New York, 2002; pp 315–324.

<u>NO. OF COPIES</u>	<u>ORGANIZATION</u>	<u>NO. OF COPIES</u>	<u>ORGANIZATION</u>
1 (PDF ONLY)	DEFENSE TECHNICAL INFORMATION CTR DTIC OCA 8725 JOHN J KINGMAN RD STE 0944 FORT BELVOIR VA 22060-6218		<u>ABERDEEN PROVING GROUND</u>
1	US ARMY RSRCH DEV & ENGRG CMD SYSTEMS OF SYSTEMS INTEGRATION AMSRD SS T 6000 6TH ST STE 100 FORT BELVOIR VA 22060-5608	1	DIR USARL AMSRD ARL CI OK TP (BLDG 4600)
1	INST FOR ADVNCD TCHNLGY THE UNIV OF TEXAS AT AUSTIN 3925 W BRAKER LN STE 400 AUSTIN TX 78759-5316		
1	US MILITARY ACADEMY MATH SCI CTR EXCELLENCE MADN MATH THAYER HALL WEST POINT NY 10996-1786		
1	DIRECTOR US ARMY RESEARCH LAB IMNE AD IM DR 2800 POWDER MILL RD ADELPHI MD 20783-1197		
3	DIRECTOR US ARMY RESEARCH LAB AMSRD ARL CI OK TL 2800 POWDER MILL RD ADELPHI MD 20783-1197		
3	DIRECTOR US ARMY RESEARCH LAB AMSRD ARL CS IS T 2800 POWDER MILL RD ADELPHI MD 20783-1197		

<u>NO. OF COPIES</u>	<u>ORGANIZATION</u>	<u>NO. OF COPIES</u>	<u>ORGANIZATION</u>
1	DIR USARL AMSRD ARL SE L D SNIDER 2800 POWDER MILL RD ADELPHI MD 20783-1197	1	DIRECTOR US ARMY AMCOM SFAE AV RAM TV D CALDWELL BUILDING 5300 REDSTONE ARSENAL AL 35898
1	HQDA DAMI FIT NOLAN BLDG WASHINGTON DC 20310-1025	1	US ARMY CRREL P DUTTA 72 LYME RD HANOVER NH 03755
1	CDR US ARMY MATERIEL CMD AMXMI INT 5001 EISENHOWER AVE ALEXANDRIA VA 22333-0001	6	US ARMY RESEARCH OFFICE A CROWSON D MANN J PRATER G ANDERSON B LAMATTINA J CHANG PO BOX 12211 RESEARCH TRIANGLE PARK NC 27709-2211
1	PEO CS&CSS PM LTV SFAE CSS LT (M114 MGR) 6501 E ELEVEN MILE RD WARREN MI 48392-5000		
2	NAVAL RESEARCH LAB R BADALIANCE CODE 6304 R MEGER CODE 6750 WASHINGTON DC 20375	1	NAVAL SURFACE WARFARE CTR TECH LIBRARY CODE B60 17320 DAHLGREN RD DAHLGREN VA 22448
1	CDR US ARMY TACOM PM GROUND SYSTEMS INTEGRATION SFAE GCSS W GSI R LABATILLE 6501 ELEVEN MILE RD WARREN MI 48397-5000	2	OFFICE OF NAVAL RESEARCH G GRAF P SCHMIDT 800 N QUINCY ST ARLINGTON VA 22217-5660
5	BENET LABS AMSTA AR CCB R FISCELLA E KATHE A LITTLEFIELD K TRUSZKOWSKA J ANDREA WATERVLIET NY 12189	6	NAVAL SURFACE WARFARE CTR J FRAYSSE CODE G33 R HUBBARD CODE G33 C PETRY R ELLIS J BEAN F BEACH DAHLGREN VA 22448
2	NAVAL AIR SYSTEMS COMMAND MATERIAL DIVISION D MOORE S CLAUSE 16906 TIDEWATER LANE HUGHESVILLE MD 20637	1	WATERWAYS EXPERIMENT D SCOTT 3909 HALLS FERRY RD SC C VICKSBURG MS 39180
		1	DARPA B WILCOX 3701 N FAIRFAX DR ARLINGTON VA 22203-1714

<u>NO. OF COPIES</u>	<u>ORGANIZATION</u>	<u>NO. OF COPIES</u>	<u>ORGANIZATION</u>
1	NASA GLENN RESEARCH CTR POWER AND PROPULSION OFFICE K MCLALLIN MS 500 103 21000 BROOK PARK RD CLEVELAND OH 44135	1	US ARMY MISSILE COMMAND AMSAM RD MG W MCCORKLE REDSTONE ARSENAL AL 35898-5240
1	OAK RIDGE NATL LAB J HANSEN MS 8051 PO BOX 2008 OAK RIDGE TN 37831-6195	3	US ARMY TACOM TARDEC AMSTA TR D J CHAPIN M TOURNER A LIJOI MS 207 WARREN MI 48397-5000
2	DIRECTOR LLNL S DETERESA M FINGER MS 313 PO BOX 808 LIVERMORE CA 94550	1	US ARMY TACOM ARDEC FSAE GCSS TMA J BENETT BLDG 354 PICATINNY ARSENAL NJ 07806-5000
4	NASA LANGLEY RESEARCH CTR AMSRD ARL VT W ELBER F BARTLETT JR T K O BRIEN W JACKSON MS 266 HAMPTON VA 23681-0001	3	US ARMY TACOM ARDEC AMSRD AAR AEW E(D) M CILLI G COLOMBO D LADD PICATINNY ARSENAL NJ 07806-5000
1	DIRECTOR DEFENSE INTELLIGNC AGCY TA 5 K CRELLING WASHINGTON DC 20310	1	US ARMY TACOM ARDEC AMSTA AR CCF A C LE PICATINNY ARSENAL NJ 07806-5000
1	CUSTOM ANALYTICAL ENG SYS INC A ALEXANDER 13000 TENSOR LN NE FLINTSTONE MD 21530	1	NSWC CARDEROCK DIVISION J SOFIA 9500 MACARTHUR BLVD WEST BETHESDA MD 20817-5700
1	DIR FOR THE DIRECTORATE OF FORCE DEVELOPMENT US ARMY ARMOR CTR COL E BRYLA FT KNOX KY 40121-5000	2	LOCKHEED MARTIN VOUGHT R BIDDLE T HOU PO BOX 650003 MS WT 21 DALLAS TX 75625-0003
1	US ARL AMSRD ARL SE RU G MCNALLY 2800 POWDER MILL RD ADELPHI MD 20783-1145		

<u>NO. OF COPIES</u>	<u>ORGANIZATION</u>	<u>NO. OF COPIES</u>	<u>ORGANIZATION</u>
8	INST FOR ADVANCED TECH UNIV OF TEXAS AT AUSTIN P SULLIVAN H FAIR K T HSIEH F STEPHANI I MCNAB C PERSAD S BLESS M ERENGIL 3925 W BRAKER LN STE 400 AUSTIN TX 78759-5316	2	SAIC G CHRYSSOMALLIS I MAY 3800 WEST 80TH ST SUITE 1090 BLOOMINGTON MN 55431
7	UNIV OF TEXAS AT AUSTIN CENTER FOR ELECTROMECHANICS J HAHNE M WERST J KITZMILLER J BENO B RECH R THOMPSON J PAPPAS PRC MAIL CODE R7000 AUSTIN TX 78712	3	SAIC B RIENSTRA A WALLS S DRATAP 8200 N MOPAC EXPRESSWAY STE 150 AUSTIN TX 78759
1	INST FOR DEFENSE ANALYSIS I KOHLBERG 1801 N BEAUREGARD ST ALEXANDRIA VA 22311	1	SAIC K A JAMISON 1247 B N EGLIN PKWY SHALIMAR FL 32579
1	UNIV AT BUFFALO SUNY AB J SARJEANT PO BOX 601900 BUFFALO NY 14260-1900	2	IAP RESEARCH INC D BAUER J BARBER 2763 CULVER AVE DAYTON OH 45429-3723
2	UDLP B GOODELL R JOHNSON MS M170 4800 EAST RIVER RD MINNEAPOLIS MN 55421-1498	1	TITAN CORPORATION T WOLFE 9244 BALBOA AVE SAN DIEGO CA 92123
1	UNIV OF TEXAS AT AUSTIN M DRIGA ENS 434 DEPT OF ECE MAIL CODE 60803 AUSTIN TX 78712	3	CURTISS-WRIGHT EMD M DEMBRAK K BERTON J HILLENBRAND CHESWICK PA 15024-1300
1	KAMAN ELECTROMAGNETICS CORP P MONGEAU 2 FOX RD HUDSON MA 01749	1	ATA ASSOCIATES W ISBELL PO BOX 6570 SANTA BARBARA CA 93160-6570
		1	DEPUTY ASST SECY FOR R&T SARD TT T KILION M FREEMAN RM 3EA79 THE PENTAGON WASHINGTON DC 20301-7100

<u>NO. OF COPIES</u>	<u>ORGANIZATION</u>	<u>NO. OF COPIES</u>	<u>ORGANIZATION</u>
1	DIR USARL AMSRD ARL WM MB A FRYDMAN 2800 POWDER MILL RD ADELPHI MD 20783-1197		W ROY J SANA D SPAGNUOLO S WALSH AMSRD ARL WM T B BURNS AMSRD ARL WM TA W GILLICH C HOPPEL M KEELE M ZOLTOSKI M NOMANDIA W BRUCHEY T WRIGHT AMSRD ARL WM TC R COATES B SORENSEN AMSRD ARL WM TE J POWELL AMSRD ARL WM TD S SCHOENFELD AMSRD ARL SE E SHAFFER
	<u>ABERDEEN PROVING GROUND</u>		
52	DIR USARL AMSRD ARL SL B AMSRD ARL WM B E SCHMIDT AMSRD ARL WM BA D LYON AMSRD ARL WM BC P PLOSTINS J NEWILL A ZIELINSKI AMSRD ARL WM BD B FORCH AMSRD ARL WM BR C SHOEMAKER AMSRD ARL WM M B FINK J MCCAULEY J BEATTY AMSRD ARL WM MA S MCKNIGHT E WETZEL P MOY AMSRD ARL WM MB A ABRAHAMIAN J BENDER T BOGETTI L BURTON W DRYSDALE D HOPKINS R KASTE T LI R EMERSON R CARTER J SOUTH E SZYMANSKI J TZENG AMSRD ARL WM MC D GRANVILLE M MAHER W SPURGEON AMSRD ARL WM MD C CHIN P DEHMER R DOOLEY S GHIORSE R LIEB		

INTENTIONALLY LEFT BLANK.